Journal of Science: Advanced Materials and Devices 7 (2022) 100463

Contents lists available at ScienceDirect

Journal of Science: Advanced Materials and Devices

journal homepage: www.elsevier.com/locate/jsamd

Original Article

Deviceful LiCl salt hydrate confinement into a macroporous silicone foam for low-temperature heat storage application

Luigi Calabrese*, Davide Palamara, Elpida Piperopoulos, Emanuela Mastronardo, Candida Milone, Edoardo Proverbio

Department of Engineering, University of Messina, Contrada di Dio Sant'Agata, 98166 Messina, Italy

ARTICLE INFO

Article history:
Received 7 July 2021
Received in revised form
2 April 2022
Accepted 11 April 2022
Available online 15 April 2022

Keywords:
Silicone foam
Salt hydrate
LiCl
Thermal energy storage

ABSTRACT

LiCl is a well-investigated salt hydrate for low-temperature thermal energy storage due to its high energy storage density (~1250 Wh/kg), which, however, suffers from deliquescence. Its hygroscopicity induces relevant issues during hydration/dehydration cycles due to water vapor mass transfer, swelling, and agglomeration. Finding a proper semipermeable container that retains the salt and allows free water vapor flow would enhance the dehydration/hydration kinetics and conversion. In this study, a new promising macro-porous LiCl filled composite foams was evaluated for storing low-temperature heat below 100 °C. Composite foams at varying salt hydrate content were prepared (0–70% wt.). The optimal formulation was addressed by coupling morphological, absorption, and energy storage density performances. The morphological analysis evidenced a relationship between foam microstructure and salt hydrate content. Hydration/dehydration measurements indicate that the composite foam allows the water vapor diffusion thanks to its interconnected microporous structure, preventing mass diffusion issues. An energy storage density of up to 665 kWh/m^3 was estimated. Furthermore, the relatively homogeneous dispersion of the salt hydrate filler in the matrix facilitates the hydration/dehydration process, leading to a notably less pronounced hysteresis area. Based on sorption, manufacturing, service, and handling feasibility, these results indicate this material as a potentially effective option for this application.

1. Introduction

Thermal energy storage (TES) is an emerging technology that proposes an efficient and effective sustainable use of solar energy [1–3]. The peak load demand can be shifted into off-peak hours using the heat energy stored by the TES units [4].

The TES systems usually applied for heating or cooling buildings are mainly based on sensible heat storage. In particular, for low-temperature sensible heat storage, water represents the common industrial option thanks to its high specific heat capacity, low cost, and environmental safety [5]. A further approach is to use latent heat storage systems where the thermal charge/discharge involves a change of the material state (e.g. liquid water/ice [6] or phase change materials – PCM [7]), using the resulting enthalpy.

In recent years, a promising approach for TES application is the thermochemical energy storage [8]. The principle is to use reversible thermochemical reactions to store heat as chemical potential. The energy charging occurs by an endothermic reaction (storing the resulting enthalpy), and the energy discharging occurs during a reverse exothermic reaction.

As thermo-reversible chemical reactions, the absorption processes in the last decade are acquiring a relevant interest in the TES field [9].

Several studies [10–12] employ water vapor as sorbate and salt hydrate (e.g., LiCl, $MgSO_4$, or $SrBr_2$) as chemical sorbents. The hydration reaction of these chemical sorbents can release a significant amount of heat, due to enthalpy energy release, compared to the physical porous sorbent materials (e.g., silica gel and zeolite). However, the hygroscopic salts induce some relevant issues during hydration/dehydration cycles related to water vapor mass transfer, swelling, and agglomeration [13].

To overcome these issues, a suitable approach is to use composite sorbents, also called selective water sorbents (SWS), or salt inside porous matrix (CSPM) [13,14]. The composite sorbents consist of two main components: the hygroscopic salt and the porous hosting matrix. Specifically, the salt crystals are dispersed in the pores or interlayer of the supporting matrix [15–19]. Thanks to preferential pathways for the water vapor flow in the porous matrix, the mass transfer and the hydration/dehydration kinetic

* Corresponding author.
E-mail address: lcalabrese@unime.it (L. Calabrese).
Peer review under responsibility of Vietnam National University, Hanoi.

https://doi.org/10.1016/j.jsamd.2022.100463

reaction are also enhanced [20]. Besides, the porous matrix acts as a container for the formed salt solution, due to the deliquescence phenomena of the salt hydrate, during the absorption process, preventing possible corrosion issues on TES plant [14,21].

Several research activities focused on composite sorbents were proposed in the literature combining different salts and solid porous hosting supports [22,23]. On this concern, the LiCl salt exhibited very promising performances for low-temperature (i.e., lower than 120 °C) TES application.

Wang and co-workers [24,25] developed composite sorbents based on silica-gel and alumina mesoporous matrix with LiCl for TES application. Complete water desorption at relatively low temperatures (in the range 60–100 °C) was evidenced showing, also, an energy storage density above 300 kWh/m^3. Although, due to the limited free internal volume of the matrix, only 40 wt.% of salt (in a silica gel matrix) could be contained, thus restraining the maximum achievable energy storage density.

A further study assessed the use of multi-walled carbon nanotubes (MWCNT) as the hosting matrix of the LiCl salt, evidenced promising kinetic performances [26]. Nevertheless, some issues related to the very low density and the not easy packing inside the reactor of this CSPM limit its applicability for TES.

A vermiculite host matrix was also proposed in the literature [13,15]. This matrix, characterized by a high specific porosity, allowed to soak almost 60% of salt inside its structure. Indeed, TES density of 2600 J/g_{ads} was achieved. However, due to the poor hydrothermal stability of the vermiculite structure, relevant issues in durability and long-term reliability of the material for TES application may occur.

Aiming to maximize the salt content and mass transport during the hydration/dehydration process, a suitable approach can be identified using macroporous cellular support [27,28]. The results, based on morphological and thermogravimetric analyses, referred to $MgSO_4 \cdot 7H_2O$ filled cellular siloxane foams, showed that a relevant hydration/dehydration capacity characterizes the composite materials compared to pure salt, preserving vapor diffusion flow, good mechanical stability [29] and good salt-matrix interfacial interaction [30]. Analogous consideration was acquired on $SrBr \cdot 6H_2O$ based silicone composite foams, although possible application limits at high salt filler contents have been highlighted [31]. Furthermore, this approach could limit both the agglomeration phenomena among the salt grains and the deliquescence issues, thus exalting the energy storage efficiency of the material [31].

In this regard, it is here proposed a deviceful LiCl salt hydrate confinement into a macroporous silicone foam semipermeable container, which retains the salt inside and at the same time allows free passage of water vapor. The hydration/dehydration performances, related to the structural and morphological characteristics of LiCl salt hydrate-filled silicone composite foam, are assessed at varying salt hydrate content (0–70% wt.). Indeed, a compelling correlation between energy storage capability and macro-microstructure of the composite is a crucial research point required to improve the knowledge on applicability issues and better tailor the material for the specific conditions of use.

Here, we aim to progress by investigating a LiCl-based silicone composite foam for its use in TES applications. With respect to previous studies on similar silicone-based systems [28–31] it is here assessed whether these macroporous structures are suitably effective even for a hydrated salt, such as LiCl, that shows a marked deliquescence phenomenon. This study represents an interesting novelty to better discriminate its potential versatility and applicability.

Specifically, the experimental characterization was designed by coupling synergistically dynamic vapor sorption (DVS) thermogravimetric measurements to assess the hydration/dehydration capacity, morphological characteristics evaluation by scanning electron microscopy (SEM), and mechanical tensile-compression tests for evaluating the structural stability of the composite. The tests were conducted on systems with different lithium chloride content (in the range 40–70 wt.%), allowing the identification of formulations potentially suitable in this application context.

2. Experimental

2.1. Materials

Poly(methylhydrosiloxane) $(CH_3(H)SiO)_n$ (PMHS), silanol terminated polydimethylsiloxane (PDMS), and bis(2-ethylhexanoate)tin were all supplied by Gelest Inc., (Morrisville, Pennsylvania, USA). Ethanol, anhydrous denatured, was purchased from Sigma Aldrich. The LiCl salt (assay >99.9%), acquired from Sigma Aldrich (St. Louis, Missouri, USA), was used as hydrated salt filler.

2.2. Preparation of composite foam

The macro-porous composite structure was obtained by a dehydrogenative coupling reaction between hydroxyl functional materials with hydride functional siloxanes that react in the presence of a metal salt catalyst involving the hydrogen evolution (that acts as a bubbling agent). In this paper, silicone foams, based on poly(methylhydrosiloxane) and silanol terminated polydimethylsiloxane mixture, filled with different amounts of the salt hydrate, were synthesized following a procedure shown in [32]. In particular, PDMS and PMHS compounds were used as monomer and hardener, respectively. Bis(2-ethylhexanoate)tin was used as catalyst. The choice to use siloxane compounds as matrix constituents in the composite foams was weighted based on their high permeability to gases and, in particular, to water vapor [33]. This way the polymeric matrix should not significantly influence the water vapor diffusion, therefore, ensuring the composite hydration/dehydration processes under realistic operating conditions. Concerning the sample synthesis procedure, the mixing of siloxane monomers was performed. The $LiCl \cdot H_2O$ salt hydrated was added under vigorous mixing until a homogenously, and a well-dispersed slurry was obtained. Different amounts of salt hydrated (40–70 wt.%) were loaded in the siloxane matrix. Ethanol was added as a solvent to allow the slurry mixing and homogenization. Afterward, the tin salt catalyst was added to activate the reaction. Finally, the foaming process was carried out by placing the slurry, activated by the catalyst, in a cylindrical mold under controlled temperature (60 °C for 24 h). Fig. 1 schematically summarize the preparation steps of the salt-silicone composite foams.

The dehydrogenative coupling reaction between slurry constituents occurs during the isothermal curing at 60 °C. In particular, the hydroxyl and hydride functional groups in PDMS and PMHS compounds, respectively, react, forming a siloxane link, Si–O–Si, that gradually leads to a tri-dimensional rubber-like silicone network. In addition, gaseous volatile hydrogen is also obtained as a reaction product and acts as a chemical foaming agent.

For the composite material design, siloxane compounds were chosen as polymeric matrix due to its high permeability to the water vapor, to prevent the obstruction of the water vapor flow toward the salt hydrate filler [33,34]. The obtained composites have been codified with the "LiCl–F" prefix, combined with a number that indicates the amount (in wt.%) of the salt hydrated, added in the polymer hosting matrix (defined as PDMS + PMHS). E.g., LiCl–F60 indicates the composite foam batch characterized by 60 wt.% of $LiCl \cdot H_2O$ filler. As a reference also a pure LiCl hydrate salt was characterized (code "LiCl–F0"). In Table 1, the

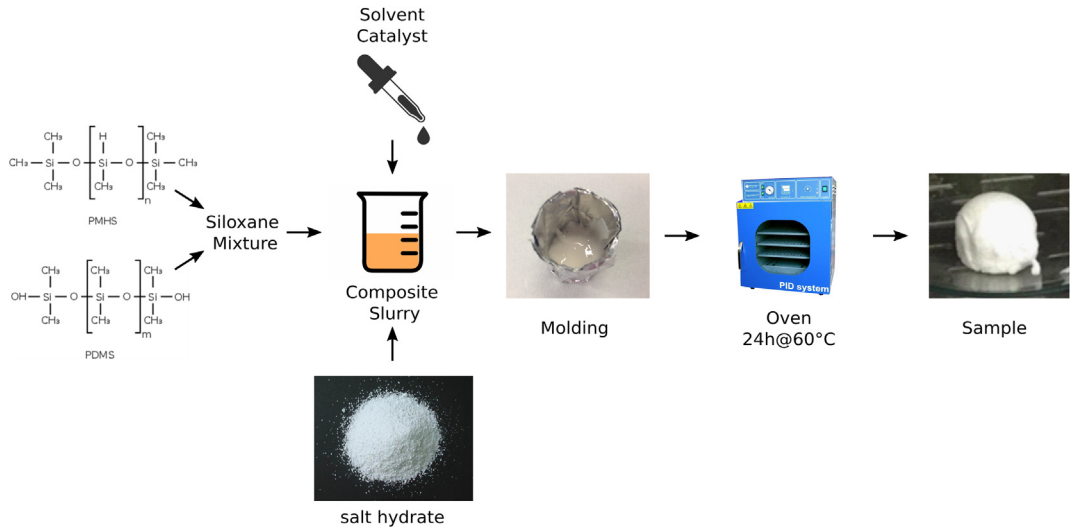

Fig. 1. Scheme of the preparation steps of the salt-silicone foams.

synthesis formulation details for all prepared foam batches were summarized.

2.3. Foam characterization

Homogeneity and voids distribution analyses were performed on the cross-sectional area of all batches, at 50× magnification, using a 3D optical digital microscope, HK-8700 (Hirox, Tokyo, Japan). Furthermore, the foam morphology was assessed using a scanning electron microscope, FEI Quanta 450 FEG (Thermo Fisher Scientific, Waltham, Massachusetts, US). A statistical analysis of bubble size distribution was carried out on all composite foam batches by digital image analysis, with the purpose of better assessing the influence of salt hydrate content on the morphological structure of the macroporous composites. In particular, bubbles distribution was digitalized, at first, by using Inkscape v.1.1 and then by ImageJ v. 1.52t software for processing and statistically analyzing the images.

The X-ray diffraction (XRD) pattern was carried out on the filled salt hydrate composite foam (LiCl—F70) to assess if the purity and crystallinity were preserved after the material synthesis. Each sample was oven-dried at 80 °C for 12 h before to carrying out the XRD measurement performed open to air at room temperature. The XRD measurements were performed using a Bruker D8 Advance diffractometer (Bruker, Billerica, MA, USA), range 2θ: 10—80°, step size: 0.010° in 0.1 s, Voltage: 40 kV, Current: 40 mA, Anode: Cu.

Compression tests were carried out on cubic-shaped specimens (dimension 10 × 10 × 10 mm^3) cut out from the large-sized molded cylinder foams. Parallelism of top and bottom surfaces was carefully checked using the previously indicated 3D optical digital microscope. Samples with parallelism tolerance larger than 3° were discarded from the analysis. Tensile tests were performed on prismatic samples with cross-sections 1 cm^2. Static tensile and flatwise compression tests were carried out using a universal testing machine, 2.5 kN Zwick Line (Zwick Roell, Ulm, Germany), equipped with a 2.5 kN load—cell. The crosshead speed was 1.0 mm/min. Three replicas for each batch were performed.

Table 1
Synthesis formulation details for all prepared foams.

Constituents	LiCl—F0	LiCl—F40	LiCl—F50	LiCl—F60	LiCl—F70
PDMS (g)	2.05	2.05	2.00	2.05	2.00
PMHS (g)	1.00	1.00	1.00	1.02	1.04
Ethanol (g)	0.50	0.50	0.55	0.70	1.3
Catalyst (g)	0.50	0.50	0.50	0.50	0.50
LiCl salt hydrate (g)	0	2.03	3.00	4.60	7.10

The hydration/dehydration capacity of the composite foams was assessed by using a thermo-gravimetric dynamic vapor system, DVS Vacuum (Surface Measurements Systems, Middlesex, UK). The instrumental setup consists of a micro-balance (precision 0.1 μg) and a water vapor pressure flow control system inside the sample holder chamber. The whole system is placed in a temperature-controlled box and maintained at a constant temperature. At first, the sample was slowly heated up to 130 °C (heating rate 1 °C/min) and kept at this temperature for about 6 h under continuous evacuation (vacuum level: 10^{-1} Pa) to degas the sample and determine its dry weight. Subsequently, a valve connecting the evaporator containing liquid water and the sample chamber was opened. An isothermal test was carried out at increasing partial pressure (P/P_0 from 0.002 to 0.9). The pressure was kept constant during each step until the sample weight achieved the equilibrium. The hydration/dehydration was calculated according to the following equation:

$$w(\mathrm{g/g}) = \frac{m\left(p_{\mathrm{H_2O}}, T_s\right) - m_0}{m_0} \quad (1)$$

where $m(p_{\mathrm{H_2O}}, T_s)$ (g), is the equilibrium weight of the sample at given water vapor pressure and temperature, m_0 (g) is the dry weight of the sample.

3. Results and discussion

3.1. Foam morphology

3.1.1. Optical observation

The 3D optical images of the cross-section area (magnification 50×) of the composite foams are shown in Fig. 2. For the sake of clear disclosure, we point out that the reported images are referred to two reference composite foam batches, LiCl—F40 and LiCl—F60, to acquire information concerning foam homogeneity at low and high salt hydrate content, respectively. Both the images are reported along the foaming direction (red arrow in each photo corner).

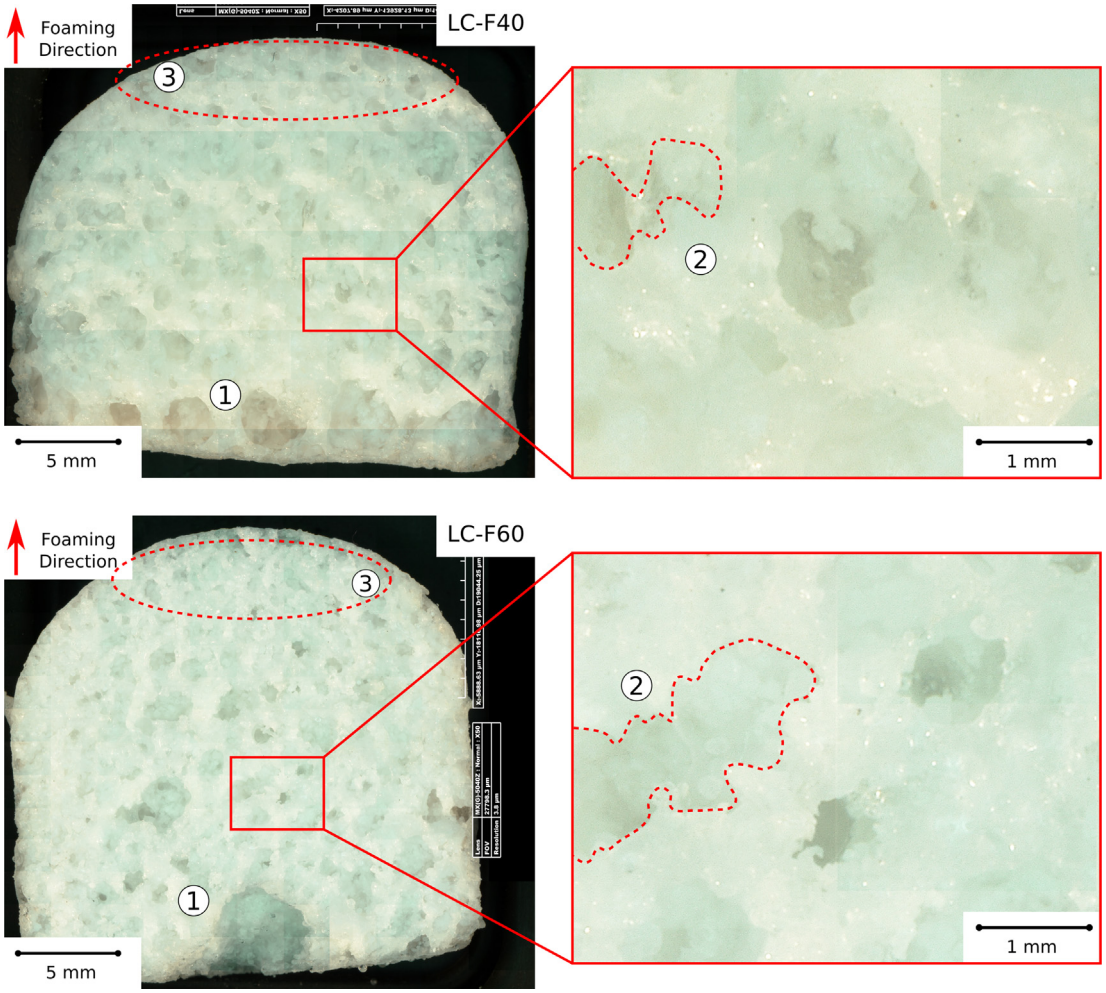

Fig. 2. 3D optical images of cross-section area of LiCl–F40 and LiCl–F60.

Both samples have a mixed open/closed macro-porous structure. Bubbles are well-interconnected to each other and uniformly distributed along the cross-section area.

The foam with higher salt content (LiCl–F60) shows a slightly smaller bubble size than the foam with the lower one (LiCl–F40). This indicates that high salt content in the composite material reduces the foaming action, limiting, indirectly, the bubbling growth phenomena. This can be ascribed to the different viscosity of the unreacted composite slurry during the preparation of the foams, which hinders the coalescence of the bubbles, leading to small size bubbles [35].

Furthermore, it can be observed that there is a gradual reduction in the size of the bubbles along the foaming direction. Large cavities of the foam on the bottom side of the specimen can be highlighted. A bimodal morphology characterizes these bubbles: i) bubbles with almost spheroidal geometry ii) bubbles of complex geometry generally branched and not regular. The former morphology, point 1 in Fig. 2, is a direct consequence of both the coalescence phenomena among bubbles and hydrogen evolution that increase the internal pressure of the bubble during the foaming process, thus leading to a bubble diameter increase [36]. The latter morphology, point 2 in Fig. 2, could be a consequence of the partial or complete interaction of neighboring cavities that aggregate, leading to new bubbles with complex geometry.

Vice versa, along the top side of the specimen, the size of the bubbles is significantly reduced. In addition, these bubbles have mainly a spheroidal shape, zone 3 in Fig. 2, indicating that the nucleation of the bubble has taken place, but the subsequent evolution and coalescence probably did not occur (or partially occurred). This results in a slightly lower level of foaming at the top of the specimen than at the bottom side.

Additionally, the salt hydrate grains are distinguishable from the matrix at higher magnification. Thus indicating, differently from zeolite–siloxane composite foams [33], a low chemical interaction between the salt hydrate and the siloxane matrix. The salt is confined within the macroporous structure without an evident chemical connection with the polymer matrix interface. Indeed, the bubbles are well defined, and their interconnection is perceived. This behavior is identifiable for composite foams both at low and high salt hydrate content. During the foaming, a progressive coalescence phenomenon among the bubbles takes place. This leads to the formation of interconnected micro- and macro-channels that allows the generation of a three-dimensional network of contiguous preferential paths for the water vapor diffusion, fundamental for the hydration and dehydration of the salt.

3.1.2. *Scanning electron microscopy observation*

Scanning Electron Microscopy analysis was carried out in order to assess the salt distribution and filler matrix interaction in the composite foams. Fig. 3 shows the micrograph of LiCl–F40 sample bottom and top sides. Moreover, punctual EDS spectra on salt filler (P1 point) and pure silicone matrix (P2 point) are added.

The salt hydrate filler is well dispersed and embedded in the silicone matrix. Due to the high filmogeneity of the PDMS matrix, the salt hydrate grains can be locally encapsulated in the matrix, thus limiting the risk of its loss while handling or during hydrothermal cycles. Indeed, this can be addressed by evaluating the EDS spectrum of P1 point, where the characteristic silicone peaks, although depressed, are still evident. On the other hand, the chlorine peak can still be observed examining P2 point, relating to the silicone part of the foam.

Furthermore, no evidence of macrocracks or defects can be observed. The cell walls are regular and homogenous with a thickness that varies comparing the bottom and the top sides due to the different microporous microstructure. The cross-section of the cell wall is homogenous without evident defects or cracks. Few voids can be detected in the matrix, probably generated during the physical or chemical foaming process [33].

Comparing the bottom and top side of the sample morphology, a slight microstructural and cell voids dimension difference in the foam is confirmed. However, this did not affect the distribution of the hydrated salt. As qualitatively identifiable in my morphological analysis, this latter remains quite homogeneous and well-integrated into the siloxane matrix without macroscopic heterogeneity or large discontinuity in its dispersion.

3.1.3. Statistical analysis

Fig. 4 shows the evolution of the average bubble diameter and circularity (calculated as $4 \cdot \pi^* (A / P^2)$ where A and P are the bubble area and diameter, respectively) in the composite foams at increasing salt hydrate content. As a reference, results referred to unfilled foam (LiCl–F0; 0% salt hydrate content) are also added.

The LiCl content significantly influences the average bubble size diameter in the foam. The addition of 40 wt.% of filler reduces about 22% of the bubble diameter. A further increase in the salt hydrate content implies a gradual decrease in the average size of the bubbles. Although a significant effect is observed for high salt contents

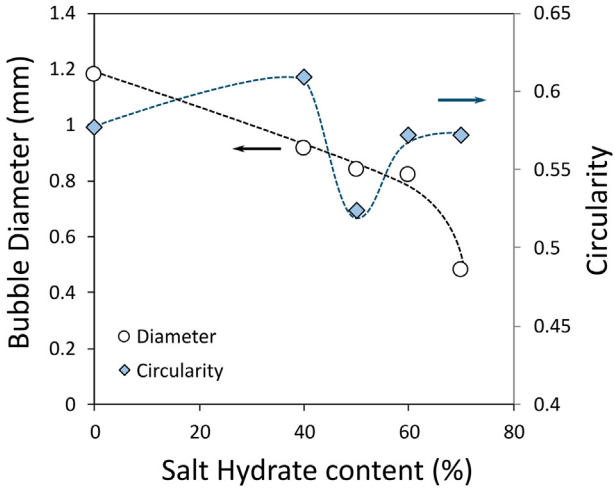

Fig. 4. Bubbles diameter and circularity at increasing salt hydrate content.

(70 wt.% of salt, LiCl–F70) for which a sharp reduction in the size of the bubbles occurred (almost 60% of the unfilled foam). At the same time, concerning the bubble circularity, a minimum is observed at intermediate salt hydrate content.

In Table 2, the average bubble diameter (d_B), densities, and porosity of the foam were calculated for all composite foams at varying salt content. The porosity of the composite foam was calculated according to the following equation:

$$P_F = 1 - \frac{\rho_F}{\rho_C} \quad (2)$$

where ρ_F and ρ_C are the apparent and solid density of the composite foam, respectively. The former was determined as the weight to

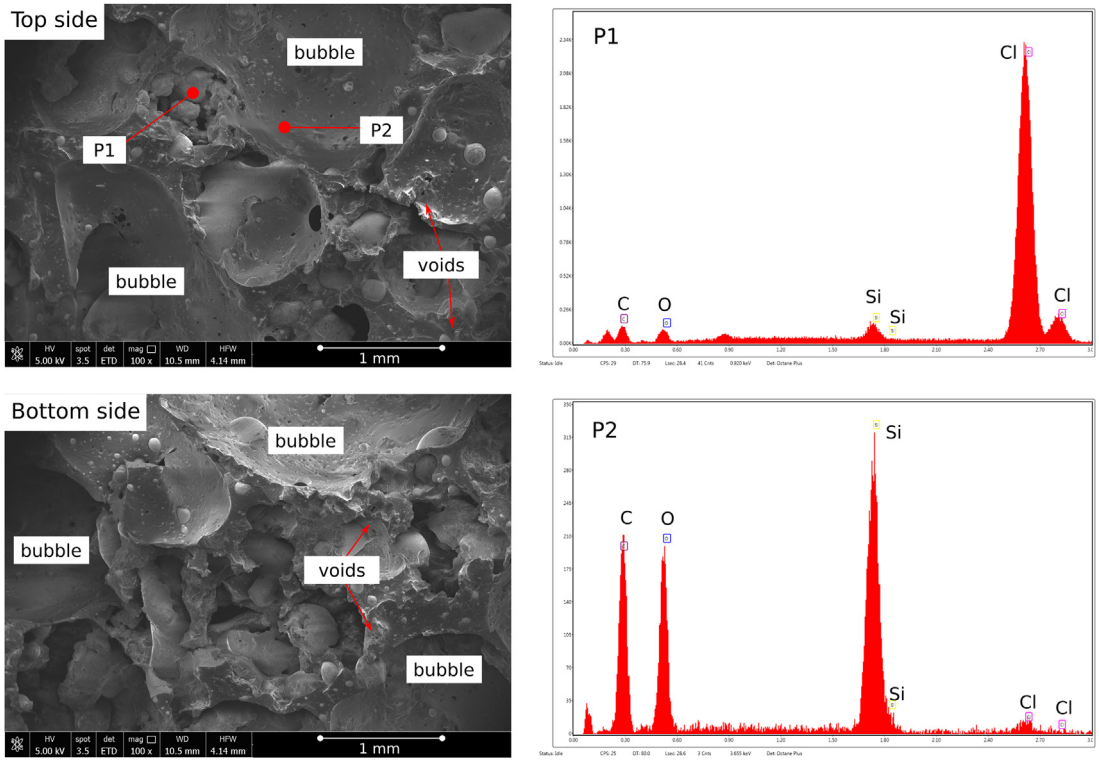

Fig. 3. Micrograph and EDS spectra in the top and bottom side of LiCl–F40 sample.

Table 2
Bubble diameter, apparent and solid density, and porosity of the composite foams.

		LiCl−F0	LiCl−F40	LiCl−F50	LiCl−F60	LiCl−F70
d_B	mm	1.18	0.92	0.84	0.82	0.48
ρ_F	g/cm^3	0.280	0.628	0.634	0.657	0.761
ρ_C	g/cm^3	0.969	1.094	1.126	1.157	1.189
P_F		0.71	0.52	0.44	0.43	0.36

volume ratio. The latter was calculated applying the mixture rule by using the constituent content in the composite foam.

As the salt hydrate content increases, an increment in the bulk density is observed together with the bubble size reduction. The unfilled siloxane foam (LiCl−F0) showed a cell size of 1.18 mm and an apparent density of 0.280 g/cm^3 (foam porosity equal to 0.71). Instead, composite foam with the highest salt content (LiCl−F70) exhibited an average bubble size of about 0.5 mm and apparent density of 0.761 g/cm^3, about 270% higher than LiCl−F0. As expected, the foam porosity, P_F decreases at increasing salt content. The composite foams with intermediate salt content exhibited an almost compatible foam porosity. While, the composite foam constituted by a high filler content (LiCl−F70) shows a very low porosity (about 50% of unfilled batch, LiCl−F0), thus confirming that a less effective foaming process occurred for this batch.

This can be explained considering that in foams with a low filler content, a large number of bubbles can complete the coalescence phase, resulting in a morphological structure with large circular bubbles. Instead, in foams with a high LiCl content, few bubbles have the possibility of interacting and coalescing due to the high viscosity of the composite slurry. Consequently, mainly small circular-shaped bubbles are observed. On the other hand, at an intermediate filler content, there is a mixed condition. Not all bubbles are able to complete the coalescence process. Therefore, at the end of the siloxane crosslinking, the matrix solidifies, and the bubbles remain interconnected with a non-regular geometry (and low circularity) correlated to the uncompleted coalescence [32]. This phenomenon is even more complex in consideration of the growing evolution of the bubbles. These dynamically grow and evolve, moving from the base of the mold towards the top. In fact, as evidenced by optical microscopy images (Fig. 2), a heterogeneous cells distribution along the foaming direction can be identified. In this context, Fig. 5 summarized the average bubble diameter at varying positions (top, middle, and bottom) in the sample along the foaming direction.

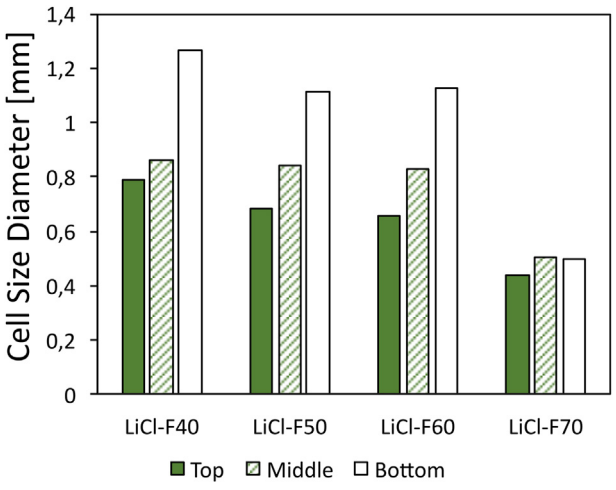

Fig. 5. Bubble diameter at the varying location along the foaming direction.

The low salt content foams (LiCl−F40, LiCl−F50, and LiCl−F60) show considerable heterogeneity in bubble distribution. In particular, the LiCl−F40 foam exhibits large bubbles mainly at the base (average size greater than 1.2 mm), indicating that the coalescence phenomenon has affected this region in a very marked way. Conversely, the middle and top areas show a very similar average size close to 0.8 mm (about 35% lower than the top side). Foams with higher hydrated salt content (LiCl−F50 and LiCl−F60) evidenced a progressive reduction of the gap between the bottom and middle sides. The size of the bubbles in the top zone is the lowest one. These results confirm the limited coalescence phenomenon affecting these batches. A totally different distribution was detected for the LiCl-F70 batch. Coalescence was significantly hindered for the foam with the highest salt content, and the dimensions of the cavities are about 0.5 mm regardless of the position along the foaming direction.

3.2. Mechanical stability

The composite foam must ensure good mechanical stability to facilitate disposal, handling, and use for TES applications. Additionally, the siloxane matrix must guarantee high flexibility to ensure the composite mechanical stability even during the deformation states induced by the hydration/dehydration process. In fact, when the lithium chloride dehydrates, with consequent loss of the water molecules, a proportional reduction in volume occurs. Similarly, during the hydration phase, a commensurate increase in volume takes place. This involves the formation of tensile and compression stresses at the interface between the hydrated salt and the matrix. A flexible matrix, contrarily to a brittle one, allows a more extensive local deformation, allowing an easier relaxation of the internal stresses during the hydration/dehydration cycles. This induces greater effectiveness and durability of the composite. In this context, composite foams with different hydrate salt content were subjected to static tensile and compression tests using a universal testing machine to evaluate the strength and stiffness of the composite foams by varying the filler content. Table 3 summarizes the compression and tensile properties of the LiCl filled siloxane foams.

The addition of the salt hydrate as filler significantly influences the mechanical performance of the foam. In particular, compression strength and stiffness (identifiable by stress at 50% of deformation, σ_{50}, and the elastic modulus E_{max}, respectively, expressed in kPa in Table 3) increase with the LiCl content. Above 40% of filler content (LiCl−F40 foam), the stiffness is 10 times greater than that observed for the unfilled one (LiCl−F0). A further increase in the salt content leads to a progressive increase of mechanical performance, reaching an elastic modulus equal to 215.23 kPa (and σ_{50} equal to 96.25 kPa) for LiCl−F70 batch. The stiffening of the composite structure is further confirmed by the reduction in deformation upon densification, ε_{dens}, for high hydrated salt content, indicating a lower tendency to suffer high deformation states for these batches. Similar consideration can be acquired by evaluating

Table 3
Compression and tensile properties of the LiCl composite foams.

	Compression test			Tensile test	
	E_{max} (kPa)	$\sigma_{50\%}$ (kPa)	ε_{dens} (%)	σ_{max} (kPa)	ε_{max} (%)
LiCl−F0	6.2 ± 1.1	7.2 ± 1.4	89.9 ± 2.0	14.4 ± 1.8	45.09 ± 3.1
LiCl−F40	72.5 ± 6.4	23.6 ± 3.1	88.6 ± 3.8	17.0 ± 3.3	45.08 ± 6.1
LiCl−F50	78.5 ± 12.5	26.2 ± 2.7	86.5 ± 1.8	21.3 ± 4.5	44.09 ± 4.4
LiCl−F60	119.0 ± 21.9	46.9 ± 3.4	80.4 ± 3.9	26.3 ± 2.1	43.77 ± 2.9
LiCl−F70	215.2 ± 21.1	96.2 ± 16.2	76.2 ± 3.3	27.6 ± 3.6	39.40 ± 5.2

the tensile properties of the composite foams at increasing salt content. In Table 3 σ_{max} and $\varepsilon_{max,}$ indicating the maximum stress (expressed in kPa) and deflection (expressed in %) under tensile test, respectively, are listed at increasing salt content in the composite foam. These results are also amplified by the foam microstructure modification induced by filler content addition [37]. A foam morphology with a small bubble size and high wall thickness promotes high strength and stiffness. Although for composite foams with high salt content, the increase in the tensile strength is less significant than compression one, probably due to a larger presence of micro-defects, which represent trigger points for the sample fracture due to tensile activation and propagation of cracks.

Summarizing, filled PDMS foams exhibited better mechanical characteristics (e.g., dimensional stability, stiffness, strength) than unfilled foam. The addition of salt hydrate powder as filler in the siloxane composite foam improves the mechanical properties in two ways: the filler acts as reinforcement, allowing an increase of the composite material strength, and at the same time, it favors mechanical and morphological stable microstructure [36].

3.3. Microstructural analysis (XRD)

Preliminarily, in Fig. 6, the X-ray diffraction pattern of LiCl filled composite foam (LiCl–F70) at 25 °C open to air, after drying overnight at 80 °C, is reported. The peaks of cubic anhydrous LiCl salt are clearly identifiable (2θ: 29.93°, 34.82°, 50.04°, 59.44°, 62.38°, 73.45°, PDF 00-004-0664) [38]. At the same time, the peaks related to the tetragonal hydrated lithium chloride LiCl·H_2O (2θ: 23.08°, 32.78°, 40.44°, 47.31°, 58.76°, 68.90°, 78.87°, PDF 00-022-1142) are visible [39]. This indicates that the anhydrous phase remains stable also at room temperature after the dehydration process. This behavior can be related to the slow structural reorder rate from the anhydrous cubic state to the hydrated tetragonal one. Furthermore, the presence of peak of LiCl·H_2O suggests that the material is sensitive to hydration phenomena occurred already during the measurement set-up, after the dehydration step. The patter has a sharp background related to the amorphous silicon matrix. Although the peaks appear sharp and narrow indicating the high degree of crystallization of the LiCl phase.

3.4. Hydration/dehydration behavior (DVS)

The water vapor sorption isotherms (30 °C) of composite foams at varying salt content are shown in Fig. 7. This isothermal condition was chosen considering the discharge temperature of a storage system in operating conditions to preliminary screen the composite material performance.

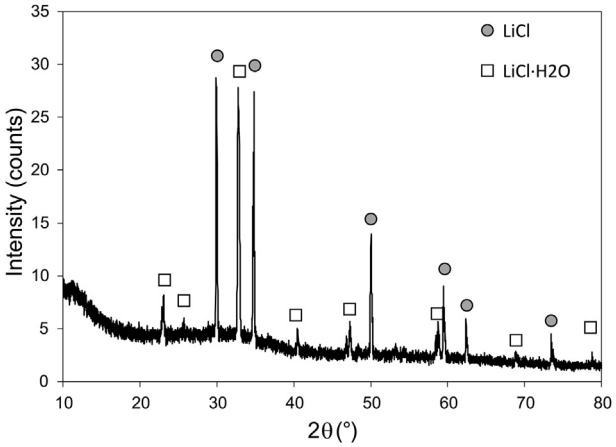

Fig. 6. XRD pattern of LiCl filled composite foam (LiCl–F70) in air at 25 °C.

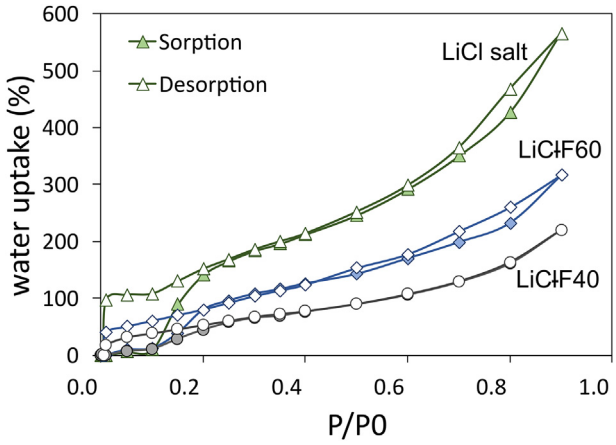

Fig. 7. Water vapor sorption isotherms of the LiCl composite foams at 30 °C. Full and empty markers for sorption and desorption branches, respectively.

As a reference, pure LiCl hydrate salt and unfilled foam (LiCl–F0) were also investigated.

The water uptake has a progressive increase at increasing partial pressure. In particular, three stages can be identified [24]:

- At low partial pressure, lower than 0.10 P/P_0, all samples do not evidence a water uptake. The curves are almost flat and near zero.
- At intermediate partial pressure, in the range 0.10–0.6, at first a sharp increase in the range 0.10–0.20 P/P_0 is observed. Afterward, a quite linear water uptake was observed from ~20 wt.% to ~100–300 wt.% (depending on the evaluated batch). The curve trend has a slight slope indicating a slow rising rate of water uptake in this range.
- Finally, a sharp increase in hydration capacity from 100 to 300 wt.% up to 550 wt.% (for pure LiCl salt hydrate) occurs.

Regarding the pure salt, a local slight hysteresis loop at a relative pressure range of 0.6–1.0 was observed. This behavior is clearly associated to the amount of salt in the composite foam, indeed, the hysteresis is less noticeable for LiCl–F40 sample. Instead, at low P/P_0 range, a second hysteresis is observed that could be related to mono- and multi-layer adsorption.

Expectedly, all the composite foams have a lower water vapor sorption capacity compared with pure LiCl salt. Although, the absorption capacity increases at increasing salt content, indicating an almost regular proportionality between salt content in the composite foam and maximum hydration. Their trend does not show a hysteresis at high partial pressures. Instead, the absorption capacity is negligible at low partial pressure, and a relevant gap at about 0.1 P/P_0 is identifiable.

These results suggest that all LiCl filler participates in the hydration/dehydration process. Taking into account the energy storage density (ESD) of the salt hydrate (~1250 Wh/kg), it is possible to estimate, based on the mixture rule of the composite, an ESD value of about 500–875 Wh/kg depending on the amount of salt in the composite. Considering the foam density reported in Table 2, the volume ESD of the composite foams varies in the range 315–665 kWh/m^3. The encapsulation of a high amount of salt in the macroporous silicone foam container allows obtaining EDS values about double compared to conventional LiCl composites [14,24], providing an effective potential use in TES applications.

In order to better discriminate the differences among all batches at increasing salt content and the initial hydration of anhydrous LiCl salt, Fig. 8a shows the evolution of the water uptake in the relative humidity range 0–25%. The water uptake was normalized to the salt hydrate content in the composite foam.

The desorption process of $LiCl \cdot H_2O$ crystals consists of two steps:

$$LiCl \cdot xH_2O\ (l) \overset{heat}{\rightarrow} LiCl \cdot H_2O\ (s) \overset{heat}{\rightarrow} LiCl(s) + H_2O\ (g) \quad (3)$$

The first step is related to the formation, at low temperature, of solid salt monohydrate $LiCl \cdot H_2O$ starting from $LiCl \cdot H_2O$ solution (deliquescence state). The second step leads to the formation of the solid LiCl salt crystals and the complete dissociation of water.

The different behavior of the isothermal curve for the composite foam can be related to the different mechanisms that occur during the composite adsorbent hydration process. Initially, (i) the salt hydrates due to a physical adsorption mechanism, namely, the water vapor interacts with the LiCl crystals due to the van der Waals force that directs the water vapor flow inside the salt grain. Subsequently, (ii) the hydration reaction of the LiCl sorbent occurs (chemical adsorption). This mechanism begins as soon as the water vapor interacts with the surface of the lithium chloride crystals. This transition can occur consequentially to physical adsorption, depending on the reaction kinetics of the process. Finally, (iii) LiCl solution is formed. When the water vapor partial pressure reaches the hydration reaction equilibrium pressure, the deliquescence phenomenon takes place. The hydrated salt continues to adsorb water vapor because of LiCl diluted solution formation. This process is coupled to a significant volume increase of the liquid phase, triggering leakage phenomena when the volume of the LiCl solution exceeds that of the cavity at the threshold relative pressure [40]. These are observed locally on the surface of the composite foam in correspondence to some external pores. From weight measurements, it is clear that the salt content that can accidentally be released during hydration/dehydration cycles is about 2.5 ± 1.35%.

In the sorption step, at low P/P_0 (<0.15) LiCl based composites exhibit a very low water uptake (Fig. 8a). At increasing relative humidity, the LiCl salt reacts with water, triggering its hydration with the formation of hydrated $LiCl \cdot H_2O$ (the dehydrated–hydrated transition hydrate salt induces a theoretical water uptake of 42.5%). This stage is related to a steep increase in the water uptake trend. A further rise in P/P_0 reveals a water uptake step on sorption isotherms ($P/P_0 \sim 0.15$). At increasing humidity, the deliquescence of the salt hydrate occurs, with the gradual increase in the uptake above the threshold value of 42.5% (referred to $LiCl \cdot H_2O$ hydration contribute), as a consequence of the progressive dilution of the concentrated LiCl solution ($P/P_0 \geq 0.20$).

Conversely, during the desorption process (Fig. 8b), all samples more difficulty dehydrate. The transition from the salt solution state to solid LiCl crystals takes place only for $P/P_0 < 0.05$, as a consequence of the deliquescence issues related to this salt hydrate [41].

A large hysteresis cycle between hydration and dehydration indicates that the salt crystals are agglomerated and hardly evolve into the liquid state and vice versa. On the other hand, a narrower hysteresis cycle can be associated to a better dispersion of the salt, which distributed in smaller lumps has a greater tendency to undergo a gradual process of hydration and dehydration. These aspects are summarized in Fig. 9, where a schematization of hysteresis evolution on the composite foams at decreasing salt hydrate is reported.

The macroporous composite foam allows water vapor diffusion within the interconnected channels, limiting the mass diffusion issues. In addition, the homogeneous dispersion, without agglomerates, of the hydrated salt within the matrix facilitates the hydration/dehydration process within the bulk, leading to a much less pronounced hysteresis area. The lower the salt content of the composite foam, the more marked this behavior is due to the better filler dispersion in the composite structure.

In this context, in agreement with the morphological characterization, the LiCl–F40 sample shows a better predisposition to hydration/dehydration cycles, being supported mainly by a lower mechanical stiffness. This makes the investigated system an excellent alternative to current solutions for thermal energy storage applications.

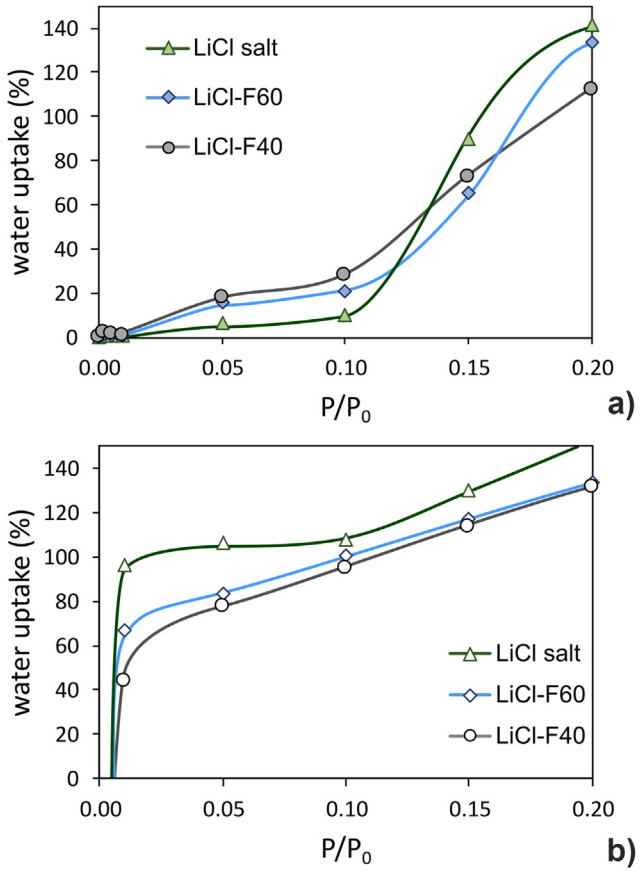

Fig. 8. Water vapor sorption isotherms of the LiCl composite foams at 30 °C in the P/P_0 range 0.0–0.2 during a) hydration and b) dehydration stages.

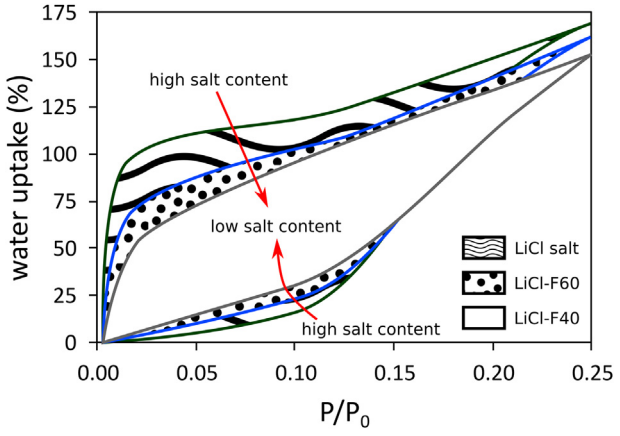

Fig. 9. Scheme of de/hydration hysteresis at varying salt content in the composite foams.

Based on the observed promising results, future works will aim at better discriminating the deliquescence phenomenon of the salt hydrate in the composite foam coupled with a more targeted evaluation of the durability to hydrothermal cycles will be developed. These further studies may give greater clarity on the value of this class of material in this research context.

4. Conclusions

A novel LiCl salt hydrate confinement into a macroporous silicone foam for low-temperature heat storage application ($\leq$100 °C) is proposed here. Composite foams at different salt hydrate content were prepared (0–70% wt.). The hydration/dehydration behavior correlated to the structural and morphological characteristics of LiCl salt hydrate-filled silicone composite foams has been assessed.

Morphological analysis evidenced a relationship between foam microstructure and salt hydrate content. Composite foams with low salt content (LiCl–F40, LiCl–F50, and LiCl–F60) exhibit a heterogeneous bubble distribution. This behavior is more evident for LiCl–F40 foam that shows bubbles larger than 1.2 mm mainly at the base, indicating a relevant coalescence phenomenon. Instead, in the LiCl–F70 batch, coalescence was significantly hindered, and the bubble size is characterized by an average diameter equal to 0.5 mm regardless the location along the foaming direction. The LiCl–F50 showed an intermediate microstructure with an interconnected open closed microstructure.

Furthermore, hydration/dehydration measurements show that the composite foam allows water vapor diffusion, thanks to its intrinsic interconnected microporous structure, limiting the mass diffusion issues. The maximum water uptake is compatible with the salt hydrate content in the composite foams, indicating that the sorbent filler actively contributes to the hydration/dehydration process, thus indicating an energy storage density up to 875 Wh/kg (665 kWh/m^3) almost double compared to conventional LiCl composites.

Pure salt hydrate exhibits a large hysteresis cycle between hydration and dehydration, indicating that the salt crystals are agglomerated and more difficulty evolve into the liquid state and vice versa. On the other hand, low LiCl content foams (LiCl–F40 and LiCl–F50) showed a narrower hysteresis cycle, correlated to a better salt dispersion in smaller lumps, which has a larger predisposition to undergo a gradual process of hydration and dehydration.

Declaration of competing interest

The authors declare that they have no known competing financial interests or personal relationships that could have appeared to influence the work reported in this paper.

Acknowledgments

This research follows from Project "NAvi efficienti tramite l'Utilizzo di Soluzioni tecnologiche Innovative e low Carbon (NAUSICA)", ARS01_00334, (M.I.U.R. – PON 2014/2020).

References

[1] L.F. Cabeza (Ed.), Advances in Thermal Energy Storage Systems, Elsevier, 2021, https://doi.org/10.1016/c2019-0-00061-1.
[2] V. Palomba, A. Frazzica, Recent advancements in sorption technology for solar thermal energy storage applications, Sol. Energy 192 (2019) 69–105, https://doi.org/10.1016/j.solener.2018.06.102.
[3] E.M. Candida Milone, Yukitaka Kato, Thermal energy storage with chemical reactions, in: Recent Adv. Mater. Syst. Therm. Energy Storage — an Introd. to Exp. Charact. Methods, 2019, pp. 15–32, https://doi.org/10.1007/978-3-319-96640-3.
[4] S. Kalaiselvam, R. Parameshwaran, Applications of thermal energy storage systems, in: Therm. Energy Storage Technol. Sustain., Elsevier, 2014, pp. 359–366, https://doi.org/10.1016/b978-0-12-417291-3.00015-3.
[5] F. Hussain, M.Z. Rahman, A.N. Sivasengaran, M. Hasanuzzaman, Energy storage technologies, in: Energy Sustain. Dev. Demand, Supply, Convers. Manag., Elsevier, 2019, pp. 125–165, https://doi.org/10.1016/B978-0-12-814645-3.00006-7.
[6] C.T. Wu, C.L. Feng, Y.H. Tsai, Application of an ice thermal energy storage system as ways of energy management in a multi-functional building, J. Renew. Sustain. Energy 7 (2015), 023107, https://doi.org/10.1063/1.4913646.
[7] Y.B. Tao, Y.L. He, A review of phase change material and performance enhancement method for latent heat storage system, Renew. Sustain. Energy Rev. 93 (2018) 245–259, https://doi.org/10.1016/j.rser.2018.05.028.
[8] H. Jarimi, D. Aydin, Z. Yanan, G. Ozankaya, X. Chen, S. Riffat, Review on the recent progress of thermochemical materials and processes for solar thermal energy storage and industrial waste heat recovery, Int. J. Low Carbon Technol. 14 (2019) 44–69, https://doi.org/10.1093/ijlct/cty052.
[9] R.J. Clark, A. Mehrabadi, M. Farid, State of the art on salt hydrate thermochemical energy storage systems for use in building applications, J. Energy Storage 27 (2020) 101145, https://doi.org/10.1016/j.est.2019.101145.
[10] V. Mamani, A. Gutiérrez, S. Ushak, Development of low-cost inorganic salt hydrate as a thermochemical energy storage material, Sol. Energy Mater. Sol. Cells 176 (2018) 346–356, https://doi.org/10.1016/j.solmat.2017.10.021.
[11] B.K. Purohit, V.S. Sistla, Inorganic salt hydrate for thermal energy storage application: a review, Energy Storage (2020) e212, https://doi.org/10.1002/est2.212.
[12] O. Al-Abbasi, A. Abdelkefi, M. Ghommem, Modeling and assessment of a thermochemical energy storage using salt hydrates, Int. J. Energy Res. 41 (2017) 2149–2161, https://doi.org/10.1002/er.3776.
[13] A.D. Grekova, L.G. Gordeeva, Y.I. Aristov, Composite "LiCl/vermiculite" as advanced water sorbent for thermal energy storage, Appl. Therm. Eng. 124 (2017) 1401–1408, https://doi.org/10.1016/j.applthermaleng.2017.06.122.
[14] A. Frazzica, V. Brancato, A. Caprì, C. Cannilla, L.G. Gordeeva, Y.I. Aristov, Development of "salt in porous matrix" composites based on LiCl for sorption thermal energy storage, Energy 208 (2020) 118338, https://doi.org/10.1016/j.energy.2020.118338.
[15] V. Brancato, L.G. Gordeeva, A. Sapienza, V. Palomba, S. Vasta, A.D. Grekova, A. Frazzica, Y.I. Aristov, Experimental characterization of the LiCl/vermiculite composite for sorption heat storage applications, Int. J. Refrig. 105 (2019) 92–100, https://doi.org/10.1016/j.ijrefrig.2018.08.006.
[16] A.D. Grekova, L.G. Gordeeva, Z. Lu, R. Wang, Y.I. Aristov, Composite "LiCl/MWCNT" as advanced water sorbent for thermal energy storage: sorption dynamics, Sol. Energy Mater. Sol. Cells 176 (2018) 273–279, https://doi.org/10.1016/j.solmat.2017.12.011.
[17] N. Yu, R.Z. Wang, Z.S. Lu, L.W. Wang, Study on consolidated composite sorbents impregnated with LiCl for thermal energy storage, Int. J. Heat Mass Transf. 84 (2015) 660–670, https://doi.org/10.1016/j.ijheatmasstransfer.2015.01.065.
[18] W. Li, Characterisation and Sorption Behaviour of LiOH-LiCl @ EG Composite Sorbents for Thermochemical Energy Storage with Controllable Thermal Upgradeability, 2021, p. 421, https://doi.org/10.1016/j.cej.2021.129586.
[19] Q. Miao, Y. Zhang, X. Jia, Z. Li, L. Tan, Y. Ding, $MgSO_4$-expanded graphite composites for mass and heat transfer enhancement of thermochemical energy storage, Sol. Energy 220 (2021) 432–439, https://doi.org/10.1016/j.solener.2021.03.008.
[20] K. Posern, K. Linnow, M. Niermann, C. Kaps, M. Steiger, Thermochemical investigation of the water uptake behavior of $MgSO_4$ hydrates in host materials with different pore size, Thermochim. Acta 611 (2015) 1–9, https://doi.org/10.1016/J.TCA.2015.04.031.
[21] A.G. Fernández, M. Fullana, L. Calabrese, V. Palomba, A. Frazzica, L.F. Cabeza, Corrosion assessment of promising hydrated salts as sorption materials for thermal energy storage systems, Renew. Energy 150 (2020) 428–434, https://doi.org/10.1016/j.renene.2020.01.001.
[22] S.P. Casey, D. Aydin, S. Riffat, J. Elvins, Salt impregnated desiccant matrices for 'open' thermochemical energy storage — hygrothermal cyclic behaviour and energetic analysis by physical experimentation, Energy Build. 92 (2015) 128–139, https://doi.org/10.1016/j.enbuild.2015.01.048.
[23] Q. Zhao, J. Lin, H. Huang, Q. Wu, Y. Shen, Y. Xiao, Energy & buildings optimization of thermochemical energy storage systems based on hydrated salts: a review, Energy Build. 244 (2021) 111035, https://doi.org/10.1016/j.enbuild.2021.111035.
[24] Y.N. Zhang, R.Z. Wang, T.X. Li, Thermochemical characterizations of high-stable activated alumina/LiCl composites with multistage sorption process for thermal storage, Energy 156 (2018) 240–249, https://doi.org/10.1016/j.energy.2018.05.047.
[25] N. Yu, R.Z. Wang, Z.S. Lu, L.W. Wang, Development and characterization of silica gel-LiCl composite sorbents for thermal energy storage, Chem. Eng. Sci. 111 (2014) 73–84, https://doi.org/10.1016/j.ces.2014.02.012.
[26] V. Brancato, L.G. Gordeeva, A.D. Grekova, A. Sapienza, S. Vasta, A. Frazzica, Y.I. Aristov, Water adsorption equilibrium and dynamics of LICL/MWCNT/PVA composite for adsorptive heat storage, Sol. Energy Mater. Sol. Cells 193 (2019) 133–140, https://doi.org/10.1016/j.solmat.2019.01.001.
[27] B.K. Purohit, V.S. Sistla, Crystallization of inorganic salt hydrates in polymeric foam for thermal energy storage application, J. Energy Storage 12 (2017) 196–201, https://doi.org/10.1016/j.est.2017.05.001.
[28] V. Brancato, L. Calabrese, V. Palomba, A. Frazzica, M. Fullana-Puig, A. Solé, L.F. Cabeza, $MgSO_4 \cdot 7H_2O$ filled macro cellular foams: an innovative composite

sorbent for thermo-chemical energy storage applications for solar buildings, Sol. Energy 173 (2018) 1278–1286, https://doi.org/10.1016/j.solener.2018.08.075.
[29] L. Calabrese, V. Brancato, V. Palomba, A. Frazzica, L.F. Cabeza, Magnesium sulphate-silicone foam composites for thermochemical energy storage: assessment of dehydration behaviour and mechanical stability, Sol. Energy Mater. Sol. Cells 200 (2019), https://doi.org/10.1016/j.solmat.2019.109992.
[30] E. Piperopoulos, L. Calabrese, P. Bruzzaniti, V. Brancato, V. Palomba, A. Caprì, A. Frazzica, L.F. Cabeza, E. Proverbio, C. Milone, Morphological and structural evaluation of hydration/dehydration stages of $MgSO_4$ filled composite silicone foam for thermal energy storage applications, Appl. Sci. 10 (2020) 453, https://doi.org/10.3390/app10020453.
[31] L. Calabrese, V. Brancato, V. Palomba, A. Frazzica, L.F. Cabeza, Innovative composite sorbent for thermal energy storage based on a $SrBr_2 \cdot 6H_2O$ filled silicone composite foam, J. Energy Storage 26 (2019), https://doi.org/10.1016/j.est.2019.100954.
[32] L. Calabrese, V. Brancato, V. Palomba, A. Frazzica, L.F. Cabeza, Assessment of the hydration/dehydration behaviour of $MgSO_4 \bullet 7H_2O$ filled cellular foams for sorption storage applications through morphological and thermo-gravimetric analyses, Sustain. Mater. Technol. 17 (2018), e00073, https://doi.org/10.1016/J.SUSMAT.2018.E00073.
[33] L. Calabrese, L. Bonaccorsi, A. Freni, E. Proverbio, Synthesis of SAPO-34 zeolite filled macrocellular foams for adsorption heat pump applications: a preliminary study, Appl. Therm. Eng. 124 (2017) 1312–1318, https://doi.org/10.1016/j.applthermaleng.2017.06.121.
[34] L. Calabrese, L. Bonaccorsi, A. Freni, E. Proverbio, Silicone composite foams for adsorption heat pump applications, Sustain. Mater. Technol. 12 (2017) 27–34, https://doi.org/10.1016/j.susmat.2017.04.002.
[35] L. Calabrese, L. Bonaccorsi, P. Bruzzaniti, A. Freni, E. Proverbio, Morphological and functional aspects of zeolite filled siloxane composite foams, J. Appl. Polym. Sci. 135 (2018) 45683, https://doi.org/10.1002/app.45683.
[36] L. Calabrese, L. Bonaccorsi, P. Bruzzaniti, G. Gullì, A. Freni, E. Proverbio, Zeolite filled siloxane composite foams: compression property, J. Appl. Polym. Sci. 135 (2018) 46145, https://doi.org/10.1002/app.46145.
[37] H. Yu, Z. Guo, B. Li, G. Yao, H. Luo, Y. Liu, Research into the effect of cell diameter of aluminum foam on its compressive and energy absorption properties, Mater. Sci. Eng. A. 454–455 (2007) 542–546, https://doi.org/10.1016/j.msea.2006.11.091.
[38] L.G. Gordeeva, A. Freni, T.A. Krieger, G. Restuccia, Y.I. Aristov, Composites "lithium halides in silica gel pores": methanol sorption equilibrium, Microporous Mesoporous Mater. 112 (2008) 254–261, https://doi.org/10.1016/j.micromeso.2007.09.040.
[39] E. Piperopoulos, V. Brancato, L. Gordeva, A. Grekova, C. Milone, A. Frazzica, Investigation of the cycling stability of sorbent composites for sorption thermal energy storage applications, in: ISEC Int. Sustain. Energy Conf. 2018, 3–5 Oct. 2018, Graz (Austria), 2018, pp. 381–384, https://doi.org/10.32638/proceedings.isec2018.201851.
[40] X. Zheng, T.S. Ge, L.M. Hu, R.Z. Wang, Development and characterization of mesoporous silicate-LiCl composite desiccants for solid desiccant cooling systems, Ind. Eng. Chem. Res. 54 (2015) 2966–2973, https://doi.org/10.1021/ie504948j.
[41] V. Brancato, L.G. Gordeeva, A. Caprì, A.D. Grekova, A. Frazzica, Experimental comparison of innovative composite sorbents for space heating and domestic hot water storage, Crystals 11 (2021) 476, https://doi.org/10.3390/cryst11050476.